



HAL
open science

Raman Thermometry Characterization of GeSbTe based Phase Change Materials

Akash Patil, Yannick Le Friec, Jury Sandrini, Roberto Simola, Philippe Boivin, Emmanuel Dubois, Jean-François Robillard

► To cite this version:

Akash Patil, Yannick Le Friec, Jury Sandrini, Roberto Simola, Philippe Boivin, et al.. Raman Thermometry Characterization of GeSbTe based Phase Change Materials. 28th International Workshop on Thermal Investigations of ICs and Systems (THERMINIC 2022), Sep 2022, Dublin, Ireland. pp.1-5, 10.1109/THERMINIC57263.2022.9950662 . hal-03875742v1

HAL Id: hal-03875742

<https://hal.science/hal-03875742v1>

Submitted on 24 Nov 2022 (v1), last revised 29 Nov 2022 (v2)

HAL is a multi-disciplinary open access archive for the deposit and dissemination of scientific research documents, whether they are published or not. The documents may come from teaching and research institutions in France or abroad, or from public or private research centers.

L'archive ouverte pluridisciplinaire **HAL**, est destinée au dépôt et à la diffusion de documents scientifiques de niveau recherche, publiés ou non, émanant des établissements d'enseignement et de recherche français ou étrangers, des laboratoires publics ou privés.

Raman Thermometry Characterization of GeSbTe based Phase Change Materials

Akash Patil
*Institut d'Electronique de
Microélectronique et de
Nanotechnologie**
Lille, France
STMicroelectronics
Crolles, France
akash-rajendra.patil@st.com

Yannick le-Friec
STMicroelectronics
Crolles, France
yannick.le-friec@st.com

Jury Sandrini
STMicroelectronics
Crolles, France
jury.sandrini@st.com

Roberto Simola
STMicroelectronics
Rousset, France
roberto.simola@st.com

Philippe Boivin
STMicroelectronics
Rousset, France
philippe.boivin@st.com

Emmanuel Dubois
*Institut d'Electronique de
Microélectronique et de
Nanotechnologie**
Lille, France
emmanuel.dubois@iemn.fr

Jean-François Robillard
*Institut d'Electronique de
Microélectronique et de
Nanotechnologie**
Lille, France
jean-francois.robillard@iemn.fr

Abstract— Ge-rich GeSbTe N-doped alloys present a solution for the reliability and thermal stability requirements of Phase Change Memories for embedded non-volatile memory automotive applications. The thermal performance of these memories is defined by the optimization of crystallization temperature, kinetics and thermal properties of materials and interfaces. In this work, we study the structural evolution and crystallization temperature of Ge-rich GeSbTe N-doped alloy from amorphous phase to complete crystallization by Raman spectroscopy. We highlight the beginning of crystallization process by Ge crystallization, followed by crystallization of both GeTe and SbTe related structures. Further, the sensitivity of the vibrational modes present in this ternary chalcogenide alloy to temperature and power is examined to identify potential thermometers. Finally, we present the working principle of Raman thermometry to extract the thermal conductivity aided by finite-element calculations and report the thermal conductivity of Ge-rich GeSbTe N-doped alloy.

Keywords— Phase change memories, Ge-rich GST N-doped, Raman thermometry, structure, thermal conductivity

I. INTRODUCTION

This Phase change materials are the basis of optical and non-volatile memory (NVM) storage systems due to their high optical or electrical resistance contrast upon phase transition. $(\text{GeTe})_n\text{-(Sb}_2\text{Te}_3)_m$ ternary alloy system based phase change materials are at the heart of Phase Change Memories (PCMs). PCMs are one of the most mature NVM owing to its high temperature data retention, fast read/write access, better endurance, high scalability, and ease of integration with CMOS. This has been proven by its commercial realization for storage class memory [1], automotive microcontroller [2] and smart power applications [3].

The working principle of PCM is based on reversible switching between amorphous and crystalline phases. For reversible switching, the electric pulses (SET/RESET) locally heat the material via a heater to crystallize the material or to melt quench the crystalline phase to amorphous phase. As this switching is thermally initiated, knowledge of crystallization temperature, thermal properties of materials and interfaces are key to optimize this nanoscale non-volatile memory. Also, PCMs use for automotive applications is hindered by the stringent requirements for robust high temperature operation and it challenges the materials thermal stability for data retention.

PCMs based on $\text{Ge}_2\text{Sb}_2\text{Te}_5$ (GST-225) are the widely studied and is the reference material for this technology [4]. The drawback of low crystallization temperature of 150°C for GST-225 was resolved by materials engineering to cope up with the automotive standards. This was achieved by doping it with C [5], N [6] or increasing the Ge content [7] and recently by $\text{GeSe}_{1-x}\text{Te}_x$ [8]. For the Ge-rich GST, the crystallization temperature scaled with increasing Ge-content [7] and was significantly improved over 300°C with N-doping. Ge-rich GST with N-doping (GGSTN) has been extensively studied for its crystallization kinetics [9], effect of N-doping [10] and structural evolution [11] [12]. GGSTN has proved to be a potential material for commercialization.

Also, along with the progress in materials engineering for automotive applications, it is also key to optimize the thermal budget of the PCM cell. It has been reported that a total of less than 2% of heat is used for switching the phase of the PCM cell [13]. The thermal management can be improved by knowledge of thermal properties of these newly developed chalcogenide materials and better understanding of thermal behavior of the cell. So, it is also crucial to study the thermal properties of GGSTN for optimizing PCM.

*Univ. Lille, CNRS, Centrale Lille, Junia, Univ. Polytechnique Hauts-de-France, UMR 8520 - IEMN – Institut d'Electronique de microélectronique et de Nanotechnologie, F-59000 Lille, France.

In this work, we employ Raman spectroscopy to study the structural evolution, crystallization temperature and Raman thermometry to extract the thermal conductivity of the GGSTN. The key advantages of this method over other techniques like 3- ω and TDTR for thermal characterization are that there are no device design requirements, better micrometer spatial resolution and material selectivity [14] [15]. The key requirement is that the material should have vibrational modes which are sensitive to temperature - Raman active modes [16]. Change in temperature of the material can affect the position of the Raman shift of a vibrational mode or the FWHM of the peak or its intensity. These characteristics can be used to build a thermometer. So, by using a focused laser on a Raman active material, the local temperature and thermal conductivity of the material can be extracted. This method has been widely used to study temperature dependence of different vibrational modes or to extract the thermal conductivity of materials like Graphene [17], Si [18] [14], Ge [15], SiGe [14], MoS₂ [19], WTe₂ [20], TiO₂ [21]. It is applied in this work to a chalcogenide ternary alloy for the first time for extraction of its thermal conductivity.

In the first section of this work, we give a detailed analysis of the vibrational modes present in the ternary system of GGSTN and its structural evolution for different annealing temperatures. In the second section, we introduce Raman thermometry and examine the sensitivity of the vibrational modes to temperature and power which aids the extraction of the thermal conductance of the material. Finally, we present the first results for the thermal conductivity of a GGSTN by using finite element model.

II. EXPERIMENTAL METHODS

A. Sample Preparation

The Ge-rich GST N-doped (GGSTN) 200 nm thick films were deposited by physical vapor deposition on 300 mm silicon (100) wafers using an industrial tool. The GGSTN thin films were capped by a 45 nm Silicon Nitride thin film to avoid oxidation. This thickness of SiN was selected to enhance the absorbance of laser in GGSTN thin film.

B. Characterization Methods

The samples were annealed at temperatures ranging from 350°C to 500°C for 5 mins under N₂ gas flow using a Rapid Thermal Annealing setup, JIPILECTM. Raman spectra of all samples was acquired using a HoribaTM Labram HR using a 473 nm continuous wave diode pumped laser with an 1800 l/mm grating. The laser emission was focused on the sample using a long distance 100x objective with numerical aperture of 0.5. The maximum power of the laser is 26mW. A continuously variable neutral density filter was used to change the input laser power with optical density ranging from 0.04 to 4. The power was monitored by using a power meter with a photodiode sensor and a multimeter. All measurements were performed under vacuum to avoid convective losses using a LINKAM HFS350-PB4 with liquid N₂ temperature-controlled stage, LINKAMTM. Thermalization of the sample and chamber stage was assured prior to each Raman spectra acquisition.

III. RESULTS AND DISCUSSION

A. Raman spectra of amorphous GGSTN

First, we investigate the Raman spectra of GGSTN. The Raman spectra of as-deposited GGSTN is recorded under

vacuum is presented in “Fig. 1”. Low laser power was incident on the sample to minimize the heating effect inflicted by the laser to avoid structural changes. The inset shows the Lorentzian fit of the spectra. A total of 6 peaks related to different Raman active vibrational modes present in ternary GeTe-SbTe system were identified to properly fit with the experimental Raman spectrum.

These vibrational modes are related to different species of GeTe (An), SbTe (Bn) and Ge (Cn). The modes related to GeTe are primarily based on the tetrahedral structure of type GeTe_{4-n}Ge_n. The mode present at 76 cm⁻¹ (A1) can be associated to the F2 bending modes of the GeTe₄ tetrahedra [22]. The vibrational modes at 96 cm⁻¹ (A2) and 220 cm⁻¹ (A4) can be assigned to one of the bending modes and the F2 anti-symmetric stretching mode of GeTe₄ tetrahedra, respectively [23] [24]. A weak presence of A1 corner-sharing tetrahedral units GeTe_{4-n}Ge_n (n=1,2) can be spotted at 124cm⁻¹ (A3). Further, the most prominent peak at 154cm⁻¹ (B1) is related to the stretching mode of SbTe vibrations in SbTe₃ pyramidal structure [25] [26]. The GeTe modes appear to be less sensitive to Raman scattering than SbTe modes, due to their lower polarizability in this ternary mixture. The amorphous phase is assured by the presence of the peak at 272 cm⁻¹ (C1), which is associated to longitudinal vibration modes of amorphous Ge in tetrahedral sites [27].

B. Temperature dependent structural evolution of GGSTN

After mapping the different vibrational modes present in as-deposited GGSTN, we study its structural evolution as a function of annealing temperature (“Fig. 2”). The spectra were recorded at room temperature in vacuum condition, after annealing at 300°C, 350°C, 400°C, 400°C and 500°C. Up to 300°C, all the vibrational modes assigned to this ternary system, appear to be stable with no structural changes. This indicates structural stability of the material up to 300°C, which is crucial for PCMs. Next, the phase transition takes place between 300-350°C, confirming the increased crystallization temperature. This phase transition alters the structure of the material as can be clearly depicted in “Fig. 2”. At 350°C, it begins with transition of amorphous Ge vibrations at 272cm⁻¹ to crystalline Ge vibrations at 297cm⁻¹ [27]. As the annealing temperature increases from 350°C to 450°C, the crystalline Ge peak narrows indicating complete crystallization. For GeTe_{4-n}Ge_n based vibrations, the prominent peak in amorphous phase at 96 cm⁻¹ transitions to the one at 124cm⁻¹ indicating a change in the tetrahedral structure, whereas the F2 antisymmetric tetrahedral vibration at 220cm⁻¹ completely disappears

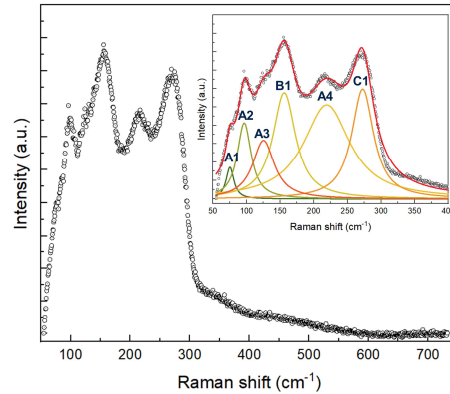


Fig. 1 Raman spectra of as-deposited GGSTN, inset: Lorentzian fit for spectra with peaks assignment

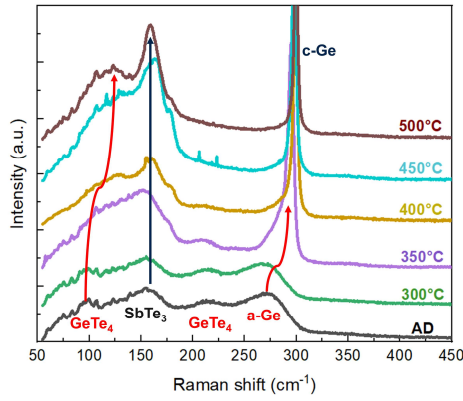


Fig 2. Raman spectra of as-deposited and annealed (300°C to 500°C) of GGSTN. Arrows indicating phase transition

indicating a reorganization in the GeTe units. In case of SbTe₃ pyramidal units, they remain stable throughout the phase transition and their crystallization is delayed. This can be observed by narrowing of the peak at 154 cm⁻¹ after 450°C.

To sum up, the crystallization begins with Ge as the peak gets narrower with increasing temperature with FWHM decreasing significantly. The delayed crystallization is a result of N-doping as it primarily bonds with Ge, inducing reduced crystallization rate and ensuring stability of the amorphous phase till higher temperature [10]. Further followed by reorganization in the structure of GeTe units. The most significant observation is the stability of SbTe₃ vibrational mode throughout crystallization.

C. Raman Thermometry

Now, we have mapped out the vibrations related to different structural units in amorphous and crystalline GGSTN Raman spectra. The basic working principle of Raman thermometry is based on temperature dependent phonon properties of the material. As the temperature of the material changes, it affects the vibrational properties of the material. This affects the position of Raman shift, line width (FWHM) and intensity of the peaks. This property is used to extract the temperature of the material. To perform thermometry, we need to identify such vibrational modes from this convoluted Raman spectra that can act as potential thermometer. For this purpose, in-situ acquisition of Raman spectra was performed for varying temperature under vacuum. Each spectrum was recorded at a step of 20°C from room temperature to 200°C and Lorentzian fitting procedure was followed. After this, calibration coefficient (χ) was extracted from fitting the modes. This parameter is defined as the change in Raman shift peak position with respect to changing temperature - ($\omega(T) = \omega_0 + \chi T$ where ω_0 is the Raman shift recorded at 0 K). For each state of GGSTN material, the vibration mode that show the highest sensitivity to temperature change (i.e. the calibration coefficient) are then selected. For amorphous GSSTN, the vibrations of SbTe₃ pyramidal structural units positioned at 154 cm⁻¹ show a calibration coefficient, $\chi = -0.01865$ cm⁻¹/K represented in “Fig. (3)”. In the crystalline GSSTN spectrum, the vibrations of crystalline Ge positioned at 300 cm⁻¹ gives $\chi = -0.01795$ cm⁻¹/K, “Fig. (4)”, consistent with previously recorded values [15]. This analysis helps us to correlate the temperature of the material to Raman shift.

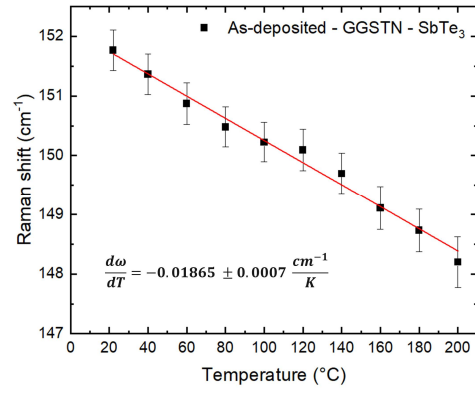


Fig 3. Calibration curve for as-deposited GGSTN – SbTe₃ mode

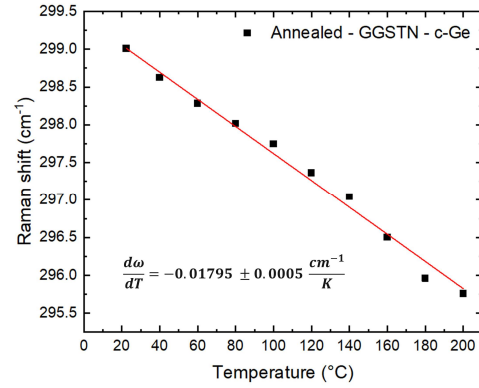


Fig 4. Calibration curve for annealed GGSTN – c-Ge mode

In the next step, the stage temperature that is the material temperature was maintained at room temperature and input power was varied. This yielded a relation between the varying input power in the material to the Raman shift. Correlating the power and temperature sensitivity, gives us the local temperature rise of the material with respect to the stage temperature (hotspot temperature) as a function of input power intensity by formulism (1) as shown in “Fig (5)”.

$$\Delta T = (\omega_p - \omega_0) / \chi \quad (1)$$

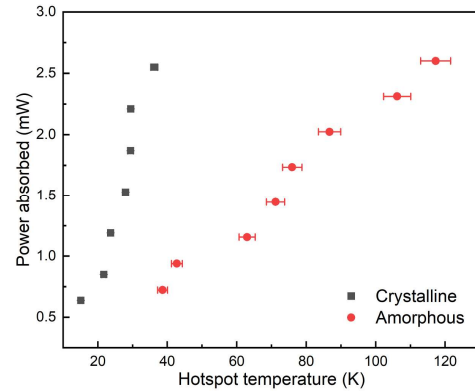


Fig. 5 Power absorbed vs local hotspot temperature of the material extracted from Raman measurements. Fit gives the thermal conductance of the material.

Where ω_p is the peak position recorded for a particular intensity of power, ω_0 is the peak position at 0K and χ is the calibration coefficient. From this we know the local temperature of the material for a specific input power and hence, the global thermal conductance (W/K) of the stack was extracted.

The global thermal conductance of amorphous GGSTN is $23 \pm 1.5 \mu\text{W/K}$ and that of crystalline GGSTN is $99.5 \pm 13.85 \mu\text{W/K}$. Here, we study the sensitivity of these specific vibrational modes related to SbTe_3 and c-Ge to temperature and power, but their behavior reflects the conductance of the global material and not only the specific material structure. Next step is to build a numerical model for extraction of the GGSTN thermal conductivity.

D. Extracting the thermal conductivity

An A finite element based numerical model was built using COMSOL 6.0. A 2D axisymmetric heat transfer model based on Fourier heat diffusion equation was built. A detailed flowchart connecting the experimental and the numerical model is represented in “Fig. (6)”. The numerical model was built under following boundary conditions. A radial Gaussian shaped power density profile was defined (2):

$$P_{gauss_abs}(r) = \frac{P_{abs}}{2 \cdot \pi \cdot R_w^2} \cdot \exp -\frac{r^2}{2 \cdot R_w^2}, \quad (2)$$

$$P_{abs} = P_{in} \cdot \text{Absorbance} \quad (3)$$

Here, the P_{abs} is the absorbed power, P_{in} is the incident power and R_w is the laser beam waist. The absorbed power was evaluated by measuring the absorbance of the as-deposited and crystalline thin film stacks using a reflectometer. A model was also built to evaluate the absorbance of GGSTN thin film [28]. The laser beam was measured using the knife-edge method. The contact between the sample and stage was assumed as an ideal heat sink with no thermal resistance. The bottom of the surface is maintained at room temperature. Power amplitude was provided as an input and GGSTN thermal conductivity was parametrized in the model.

The local hotspot temperature was extracted by defining an effective Raman temperature to replicate the experimental conditions [14].

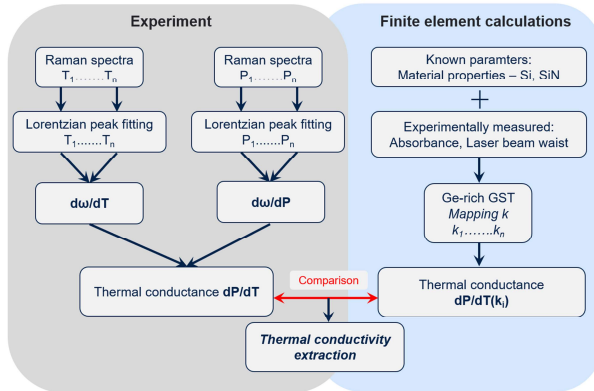


Fig. 6 Experimental workflow to obtain thermal conductance of the material for changing temperature and power, Simulation workflow to map thermal conductivity to the precise thermal conductance

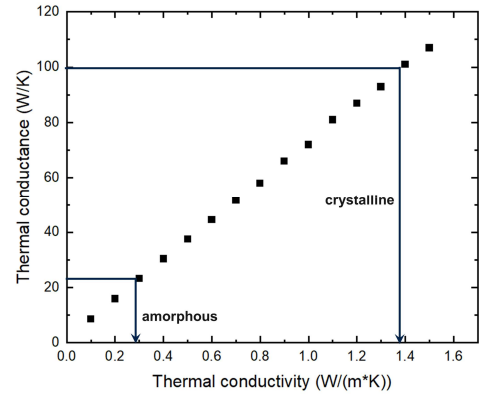


Fig. 7 Thermal conductance mapped for thermal conductivity values. Lines indicate the experimental thermal conductance to the corresponding thermal conductivity estimate.

Like experimental data, the local temperature gradient was extracted for different input power and the thermal conductance was mapped with respect to thermal conductivity of GGSTN “Fig. (7)”. The thermal conductance value extracted from simulations was compared to the experimental thermal conductance, and its coincidence gave us the precise thermal conductivity of the material. The thermal conductivity for GGSTN in amorphous and crystalline phase are $0.29 \text{ W m}^{-1} \text{ K}^{-1}$ and $1.38 \text{ W m}^{-1} \text{ K}^{-1}$ respectively.

IV. CONCLUSION

In summary, first we laid out a map of possible vibrational modes related to different structural organizations of GeTe_4 , nGe_n and SbTe_3 in GGSTN. The temperature dependent study revealed the transition in structural details from amorphous to crystalline. It begins with Ge crystallization and then the narrowing of the peak from 350°C to 450°C indicating complete crystallization. The GeTe modes switch from symmetric tetrahedral to corner sharing tetrahedral structure, whereas the SbTe_3 structure shows strong stability over the phase transition. In the next part, we were successful in identifying vibrational modes with strong dependency on temperature from a convoluted Raman spectrum. SbTe_3 mode in amorphous and c-Ge mode in crystalline phase were identified as thermometers with good calibration coefficients. Further, we demonstrated the extraction of local temperature and thermal conductance of the material. This functionality can further be helpful in thermal mapping of devices based on GST as they are being employed extensively for RF, NVM and neuromorphic devices. Finally, the precise thermal conductivity of GGSTN (amorphous and crystalline phase are $0.29 \text{ W m}^{-1} \text{ K}^{-1}$ and $1.38 \text{ W m}^{-1} \text{ K}^{-1}$ respectively) was extracted by Raman thermometry for the first time.

REFERENCES

- [1] P. Cappelletti, R. Annunziata, F. Amaid, F. Disegni, A. Maurelli, and P. Zuliani, “Phase change memory for automotive grade embedded NVM applications,” *J. Phys. D: Appl. Phys.*, vol. 53, no. 19, p. 193002, Mar. 2020, doi: 10.1088/1361-6463/ab71aa.
- [2] F. Arnaud et al., “High Density Embedded PCM Cell in 28nm FDSOI Technology for Automotive Micro-Controller Applications,” in 2020 IEEE International Electron Devices Meeting (IEDM), Dec. 2020, p. 24.2.1-24.2.4. doi: 10.1109/IEDM13553.2020.9371934.
- [3] M. Carissimi et al., “2-Mb Embedded Phase Change Memory With 16-ns Read Access Time and 5-Mb/s Write Throughput in 90-nm BCD Technology for Automotive Applications,” *IEEE Solid-State Circuits Letters*, vol. 2, no. 9, pp. 135–138, Sep. 2019, doi: 10.1109/LSSC.2019.2935874.

- [4] S. W. Fong, C. M. Neumann, and H.-S. P. Wong, "Phase-Change Memory—Towards a Storage-Class Memory," *IEEE Transactions on Electron Devices*, vol. 64, no. 11, pp. 4374–4385, Nov. 2017, doi: 10.1109/TED.2017.2746342.
- [5] Q. Hubert et al., "Lowering the Reset Current and Power Consumption of Phase-Change Memories with Carbon-Doped Ge₂Sb₂Te₅," in 2012 4th IEEE International Memory Workshop, May 2012, pp. 1–4. doi: 10.1109/IMW.2012.6213683.
- [6] H. Y. Cheng et al., "A thermally robust phase change memory by engineering the Ge/N concentration in (Ge, N)_xSb_yTe_z phase change material," in 2012 International Electron Devices Meeting, Dec. 2012, p. 31.1.1-31.1.4. doi: 10.1109/IEDM.2012.6479141.
- [7] P. Zuliani et al., "Overcoming Temperature Limitations in Phase Change Memories With Optimized Ge_xN_ySb_zTe_w," *IEEE Transactions on Electron Devices*, vol. 60, no. 12, pp. 4020–4026, Dec. 2013, doi: 10.1109/TED.2013.2285403.
- [8] M. Tomelleri et al., "Overcoming the Thermal Stability Limit of Chalcogenide Phase-Change Materials for High-Temperature Applications in GeSe_{1-x}Te_x Thin Films," *physica status solidi (RRL) – Rapid Research Letters*, vol. 15, no. 3, p. 2000451, 2021, doi: 10.1002/pssr.202000451.
- [9] E. Gomiero et al., "Crystallization Speed in Ge-Rich PCM Cells as a Function of Process and Programming Conditions," *IEEE Journal of the Electron Devices Society*, vol. 7, pp. 517–521, 2019, doi: 10.1109/JEDS.2019.2913467.
- [10] M. A. Luong et al., "Impact of Nitrogen on the Crystallization and Microstructure of Ge-Rich GeSbTe Alloys," *physica status solidi (RRL) – Rapid Research Letters*, vol. 15, no. 3, p. 2000443, 2021, doi: 10.1002/pssr.202000443.
- [11] L. Prazakova et al., "Temperature driven structural evolution of Ge-rich GeSbTe alloys and role of N-doping," *Journal of Applied Physics*, vol. 128, no. 21, p. 215102, Dec. 2020, doi: 10.1063/5.0027734.
- [12] E. Rahier et al., "Crystallization of Ge-Rich GeSbTe Alloys: The Riddle Is Solved," *ACS Appl. Electron. Mater.*, vol. 4, no. 6, pp. 2682–2688, Jun. 2022, doi: 10.1021/acsaelm.2c00038.
- [13] S. M. Sadeghipour, L. Pileggi, and M. Asheghi, "Phase change random access memory, thermal analysis," in *Thermal and Thermomechanical Proceedings 10th Intersociety Conference on Phenomena in Electronics Systems, 2006. ITherm 2006.*, May 2006, pp. 660–665. doi: 10.1109/ITHERM.2006.1645408.
- [14] B. Stoib et al., "Spatially resolved determination of thermal conductivity by Raman spectroscopy," *Semicond. Sci. Technol.*, vol. 29, no. 12, p. 124005, Nov. 2014, doi: 10.1088/0268-1242/29/12/124005.
- [15] J. Jaramillo-Fernandez, E. Chavez-Angel, and C. M. Sotomayor-Torres, "Raman thermometry analysis: Modelling assumptions revisited," *Applied Thermal Engineering*, vol. 130, pp. 1175–1181, Feb. 2018, doi: 10.1016/j.applthermaleng.2017.11.033.
- [16] S. Sandell, E. Chávez-Ángel, A. E. Sachat, J. He, C. M. S. Torres, and J. Maire, "Thermoreflectance techniques and Raman thermometry for thermal property characterization of nanostructures," *Journal of Applied Physics*, vol. 128, no. 13, p. 131101, Oct. 2020, doi: 10.1063/5.0020239.
- [17] I. Calizo, A. A. Balandin, W. Bao, F. Miao, and C. N. Lau, "Temperature Dependence of the Raman Spectra of Graphene and Graphene Multilayers," *Nano Lett.*, vol. 7, no. 9, pp. 2645–2649, Sep. 2007, doi: 10.1021/nl071033g.
- [18] T. R. Hart, R. L. Aggarwal, and B. Lax, "Temperature Dependence of Raman Scattering in Silicon," *Phys. Rev. B*, vol. 1, no. 2, pp. 638–642, Jan. 1970, doi: 10.1103/PhysRevB.1.638.
- [19] E. Yalon et al., "Temperature-Dependent Thermal Boundary Conductance of Monolayer MoS₂ by Raman Thermometry," *ACS Appl. Mater. Interfaces*, vol. 9, no. 49, pp. 43013–43020, Dec. 2017, doi: 10.1021/acsaami.7b11641.
- [20] Y. Chen et al., "Thickness dependent anisotropy of in-plane Raman modes under different temperatures in supported few-layer WTe₂," *Appl. Phys. Lett.*, vol. 119, no. 6, p. 063104, Aug. 2021, doi: 10.1063/5.0058438.
- [21] V. Zani, D. Pedron, R. Pilot, and R. Signorini, "Contactless Temperature Sensing at the Microscale Based on Titanium Dioxide Raman Thermometry," *Biosensors*, vol. 11, no. 4, Art. no. 4, Apr. 2021, doi: 10.3390/bios11040102.
- [22] K. S. Andrikopoulos, S. N. Yannopoulos, A. V. Kolobov, P. Fons, and J. Tominaga, "Raman scattering study of GeTe and Ge₂Sb₂Te₅ phase-change materials," *Journal of Physics and Chemistry of Solids*, vol. 68, no. 5, pp. 1074–1078, May 2007, doi: 10.1016/j.jpcs.2007.02.027.
- [23] K. S. Andrikopoulos, S. N. Yannopoulos, G. A. Voyiatzis, A. V. Kolobov, M. Ribes, and J. Tominaga, "Raman scattering study of the a-GeTe structure and possible mechanism for the amorphous to crystal transition," *J. Phys.: Condens. Matter*, vol. 18, no. 3, pp. 965–979, Jan. 2006, doi: 10.1088/0953-8984/18/3/014.
- [24] R. Mazzarello, S. Caravati, S. Angioletti-Uberti, M. Bernasconi, and M. Parrinello, "Signature of Tetrahedral Ge in the Raman Spectrum of Amorphous Phase-Change Materials," *Phys. Rev. Lett.*, vol. 104, no. 8, p. 085503, Feb. 2010, doi: 10.1103/PhysRevLett.104.085503.
- [25] L. Petit, N. Carlie, F. Adamietz, M. Couzi, V. Rodriguez, and K. C. Richardson, "Correlation between physical, optical and structural properties of sulfide glasses in the system Ge–Sb–S," *Materials Chemistry and Physics*, vol. 97, no. 1, pp. 64–70, May 2006, doi: 10.1016/j.matchemphys.2005.07.056.
- [26] [P. Nêmec, V. Nazabal, A. Moreac, J. Gutwirth, L. Beneš, and M. Frumar, "Amorphous and crystallized Ge–Sb–Te thin films deposited by pulsed laser: Local structure using Raman scattering spectroscopy," *Materials Chemistry and Physics*, vol. 136, no. 2, pp. 935–941, Oct. 2012, doi: 10.1016/j.matchemphys.2012.08.024.
- [27] P. Kazimierski, J. Tyczkowski, M. Kozanecki, Y. Hatanaka, and T. Aoki, "Transition from Amorphous Semiconductor to Amorphous Insulator in Hydrogenated Carbon–Germanium Films Investigated by Raman Spectroscopy," *Chem. Mater.*, vol. 14, no. 11, pp. 4694–4701, Nov. 2002, doi: 10.1021/cm020428s.
- [28] S. J. Byrnes, "Multilayer optical calculations," Mar. 2016, doi: 10.48550/arXiv.1603.02720.